Wrobel, R., & Simpson, N. (2016). Winding Loss Separation in Thermal Analysis of Electromagnetic Devices. In 2016 XXII International Conference on Electrical Machines (ICEM 2016): Proceedings of a meeting held 4-7 September 2016, Lausanne, Switzerland. (pp. 2133-2139). Institute of Electrical and Electronics Engineers (IEEE). DOI: 10.1109/ICELMACH.2016.7732817

Winding Loss Separation in Thermal Analysis of Electromagnetic Devices

Rafal Wrobel and Nick Simpson

Abstract -- **This paper investigates various winding loss separation approaches applicable to the thermal analysis of electrical machines, transformers and wound passive components. The accurate temperature prediction and identification of hot-spots within such electromagnetic devices is strongly dependent on the absolute power loss data as well as the loss distribution within the subassemblies or regions of the device. The losses within a device are often defined as the average loss over a particular region, for example, the winding loss, core loss or magnet loss. However, such a loss definition might not yield the required fidelity or resolution, particularly if localised power loss such as ac winding loss is present during device operation. To account for the inhomogeneous winding loss, a more detailed loss separation is required. In this paper, the winding subassembly is subdivided into a number of sub-regions accounting for both the active length and end-winding. Three-dimensional (3D) electromagnetic and thermal analyses are employed to give insight into the effect of the loss definition on the accuracy and validity of the temperature prediction. A hardware exemplar representative of a single-layer open-slot stator/winding subassembly has been selected for the analysis. The results suggests that detailed loss separation provides improved accuracy of the temperature predictions and hot-spots identification when compared with the more common averaged loss definition. The theoretical findings have been validated with experimental data showing close correlation.**

Index Terms—**Thermal analysis, winding power loss, end-winding power loss, loss separation, electrical machines.**

I. Introduction

THERMAL analysis of electromagnetic devices has become an essential element of the design-development process and is particularly important when considering compact, cost-effective and high-efficiency designs. A detailed insight into the thermal behaviour of a machine prior to the manufacturing stage is particularly desirable as it allows various performance measures to be assessed, for example, the power output capability and the efficiency under the intended operating conditions. However, the accuracy of thermal models is affected by numerous factors, some of which include the thermal material data, power loss data, manufacture and assembly factors, and thermal model formulation [1]-[14]. A reliable thermal model typically requires a degree of calibration and is usually informed from experiments or previous experience. This allows for the manufacture and assembly as well as the operating conditions of a machine design to be accounted for in the model definition. Such a thermal model allows for the behaviour of the machine to be predicted at various operating points providing that the appropriate power loss data is available. There are various loss components present within a machine assembly during its operation. In general, these include electromagnetic loss components when considering electromagnetic transducers such as transformers and inductors with the addition of mechanical losses and motion related electromagnetic losses when considering electromechanical machines such as motors and actuators. There is a wide body of work devoted to power loss derivation and separation using both experimental and theoretical approaches [1]-[21]. It is important to note that the experimental loss measurements on a complete device are typically limited to the absolute power loss generated and a theoretical means of separating the various loss components is usually required. In general, the power loss components required in thermal analysis are associated with the active regions of a machine, for example, the winding, stator core, rotor core, permanent magnets (PMs) among others. The power loss data derived for the individual loss components is usually averaged over a specific subassembly or region in order to simplify the loss analysis. However, such averaged loss data does not contain information regarding the localised power loss effects. The localised power losses might have a significant impact on a device's performance and thermal behaviour, thus it is crucial to understand how and when these effects should be accounted for in the design-analysis.

In this paper, the localised power loss associated with the winding subassembly is investigated in detail. The inhomogeneous distribution of loss within the winding body during its healthy operation is usually associated with the ac effects. The ac effects are particularly important, but not limited to, the design and analysis of high-speed or high-frequency machine designs [6], [9]-[14]. A hardware exemplar representative of a single-layer concentrated wound open-slot stator/winding design has been chosen in this work to demonstrate the effects. Various winding loss separation approaches with varying levels of detail are considered, where the active length and end-winding are subdivided in a number of smaller sub-regions accounting for the inhomogeneous winding loss distribution. The results suggest that the detailed winding loss separation provides improved accuracy of the temperature predictions and hot-spot identification.

II. Hardware Exemplar

A. Exemplar Construction

To show the importance of the localised winding loss in the thermal analysis of electromagnetic devices a hardware exemplar comprising of a laminated E-core and a set of

Rafal Wrobel is with the Department of Electrical Engineering, the University of Bristol, Bristol, BS8 1TR, UK and with Motor Design Ltd., Ellesmere, SY12 0EG, UK (e-mail: dr.rafal.wrobel@ieee.org)

Nick Simpson is with the Department of Electrical Engineering, the University of Bristol, Bristol, BS8 1TR, UK (e-mail: dr.nick.simpson@ieee.org).

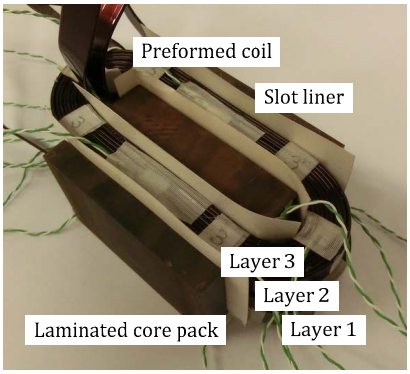

Fig. 1. Hardware exemplar representative of a single-layer concentrated wound open-slot stator/winding design prior to encapsulation

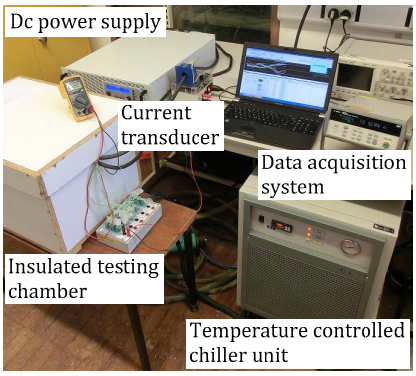

Fig. 2. An experimental setup used in dc test – impregnated hardware exemplar mounted on a liquid-cooled plate, placed in an insulated chamber

preformed multi-layer coils has been selected, Fig. 1. Such an assembly is representative of a sector of a single-layer wound open-slot stator/winding assembly. The multi-layer coil construction adopted here, allows for a varying number of coil layers with differing electrical configurations between the coil layers. In this analysis, a series connection between the coil's layers is considered only. Each of the coil layers has 10 turns of 1.1mm×10mm copper rectangular profiled conductor. The conductor arrangement within the coil layers has been chosen to exaggerate the ac winding loss effects. The laminated core pack is made of M270-35A (SiFe).

The complete exemplar assembly is instrumented with multiple type-K thermocouples located in the active length and end winding regions of each of the winding layers and also in the teeth and back iron of the core pack body. The E-core/winding assembly is encapsulated with high thermal conductivity epoxy resin. Such a construction allows for enhanced heat transfer from the winding body across the laminated core pack into the heat sink, and is representative of device designs with improved dissipative heat transfer capabilities [10], [11], [14].

B. Testing Procedure

Prior to tests the impregnated exemplar is mounted on a liquid-cooled temperature controlled plate and placed in an insulated chamber, Fig. 2. For the thermal model calibration, the winding is energised from a dc power supply, with the voltage, current and temperature data logged during duration of the test. The measurements continue until thermal equilibrium of the exemplar assembly is reached, here less than 1°C per 10mins criteria has been used. The measurements are repeated for a number of excitation current levels. For the ac power loss analysis, the exemplar is removed from the liquid-cooled cold-plate and insulated chamber and placed in an environmental chamber at a fixed temperature. The winding is energised using an ac power supply allowing to vary sinusoidal excitation current magnitude and frequency. The power loss is measured using a high-bandwidth power analyser with high-accuracy current transducer. The power loss is measured instantaneously for a fixed current magnitude over a range of frequencies at a temperature set by the environmental chamber. The total power loss data is separated into core and winding loss components using finite element analysis (FEA).

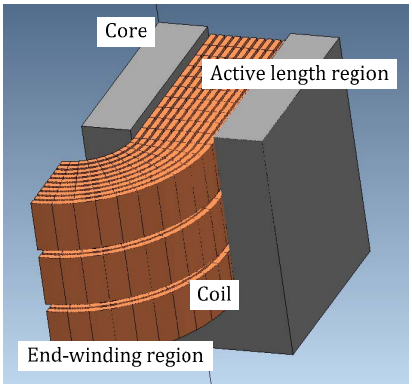

Fig. 3. 3D FE model representation of the hardware exemplar – one quarter of the complete assembly

III. FE Mathematical Models

A. Electromagnetic Analysis

To derive the localised winding power loss data, a three-dimensional (3D) FEA has been carried out. Due to symmetry, only one quarter of the hardware exemplar is analysed, Fig. 3. The individual winding conductors for the active length and end-winding sub-regions are represented within the model. An appropriate external circuit has been used to define the required electrical connections between the individual conductors and the coil layers. Such a model definition allows for the winding loss of the individual conductor to be derived and then fed into the thermal model. It is worth noting that the winding power loss data for each individual conductor gives the most detailed thermal model

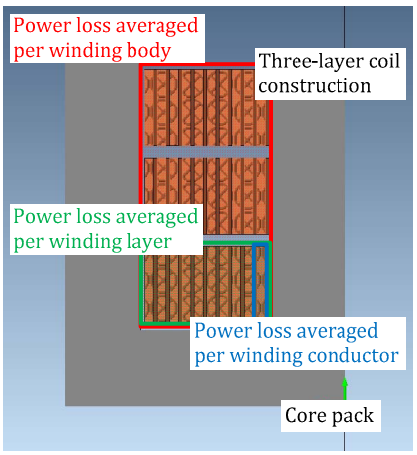

Fig. 4. Stator/winding cross-section together with averaging methods for the winding power loss at ac operation

definition considered in this work, whereas the averaged power loss data for the active and end-winding sub-regions is the commonly used coarse modelling approach, Fig. 4. Various excitation frequencies for sinusoidal excitation current and winding operating temperatures were analysed to derive a functional representation of the winding loss to be used in the thermal analysis [9], [12]. The winding loss function for an individual conductor can be written in the following form:

$$(P_{ac})_i|_T = (P_{dc})_i|_{T_0}\big(1+\alpha(T-T_0)\big) + (P_{dc})_i|_{T_0}\frac{\left(\frac{R_{ac}}{R_{dc}}\right)_i\Big|_{T_0} - 1}{\big(1+\alpha(T-T_0)\big)^{\beta_i}}, \quad (1)$$

where: subscript i refers to i-th conductor/turn within the coil, $P_{dc} = I^2R_i$, α is the temperature coefficient of electrical resistivity (for copper $\alpha = 3.93\times10^{-3}\text{C}^{-1}$), $R_{ac}/R_{dc} = P_{ac}/P_{dc}$ and represents increase of winding resistance at ac operation, T_0 is the reference temperature (usually 20°C), β is the ac winding loss fitting parameter which can be found from curve fitting (1) to ac loss data for the highest temperature considered for a device.

It has been shown in the literature that a single value β is usually adequate across a range of operating frequencies [9], [12]. Here however, β is assumed to be frequency dependant and has been derived for the consecutive excitation frequencies analysed. Fig. 5 presents an example of frequency variation of β parameter for the coarse winding loss separation with distinction to the active- and end-winding regions only. The results suggest a change of the ac winding loss character from resistance to inductance limited [20]. It is important to note that the winding loss function is derived for both the winding active length and end regions. Here, there are 60 individual loss functions with appropriate coefficients for the most detailed, per conductor winding loss representation, Fig. 4. The approach where the loss is averaged per winding layer and winding body makes use of significantly fewer individual loss functions, 6 and 2 respectively. The iron loss generated in the laminated core pack has been obtained for the same FEAs using the modified Steinmetz's equation approach and averaged over

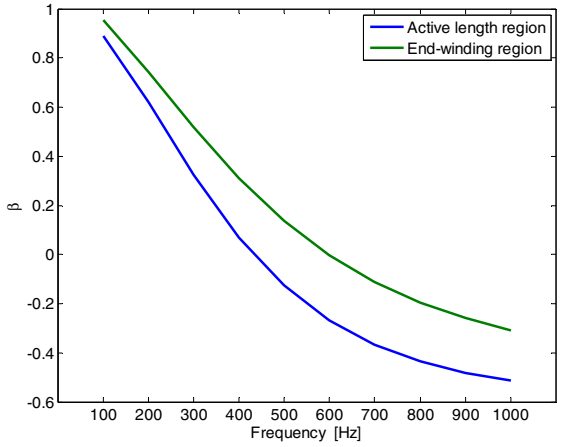

Fig. 5. Frequency variation of β coefficient for the per winding body power loss averaging including the winding active length and end regions

the core segments [3], [5], [14]. The iron loss coefficients for the Steinmetz's formula have been derived by curve fitting of the equation to specific loss data provided by the steel manufacturer.

B. *Thermal Analysis*

Thermal analysis has been performed using a fully parameterised 3D FEA model in which the temperature dependent loss within each conductor can be defined by the use of (1). The material thermal data for the laminated core pack and impregnated winding has been derived from measurements using representative material samples [7], [13].

TABLE I. MATERIAL THERMAL DATA

Model region	k_x [W/m K]	k_y [W/m K]	k_z [W/m K]
Impregnated winding	3.1	1.9	331.2
Laminated core	22.0	22.0	4.9
Epoxy resin (Epoxylite EIP 4260)	0.85	0.85	0.85
Slot liner (Nomex 410, 0.25mm)	0.13	0.13	0.13

A set of thermal conductivities used in thermal analysis is listed in table I. It is important to note that thermal data contains only the thermal conductivity as thermal steady state is of interest in this analysis. Thermal anisotropy for the assembly regions composed of multiple materials, e.g. impregnated winding and laminated core is accounted for. Here, the winding region x and y axes refer to the longer and shorter periphery of conductor cross-section respectively, whereas the z axis is aligned with conductor length. For the core pack assembly, the lowest thermal conductivity is in z axis and represents the heat path across the individual laminations. The contact thermal resistances between winding body and core pack, and core pack and cold-plate have been informed from the dc thermal tests.

To accommodate for the optional winding loss separation methods considered in the investigation, the complete winding region has been subdivided into a number of smaller sub-regions representative of individual conductor and/or winding layers for both the active- and end-winding region. The loss function (1) allows for the winding loss data to be iteratively updated with temperature without need for further derivation of the electromagnetic loss components using FEAs. In the analysed case, the main heat transfer is provided by conduction from the core/winding body into the temperature controlled cold plate, set at a fixed temperature of 20°C. The convection and radiation effects are assumed to be negligible here, and all the assembly surfaces which are not in contact with the cold-plate are assumed to be adiabatically insulated. These are set by appropriate boundary conditions in the FE thermal model.

IV. RESULTS AND OBSERVATIONS

A. *Exemplar – Winding Power Loss*

Initial loss measurements have been carried out for a number of coil variants prior to the final assembly choice and later impregnation. Here, a number of coil layers have been altered by removing the consecutive/individual coil layers

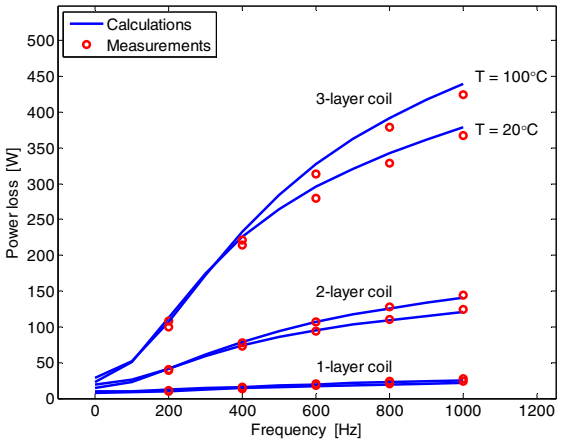

Fig. 6. Measured and calculated winding power loss versus excitation frequency for a number of coil variants and winding temperatures at $I = 40\text{A}_{\text{rms}}$

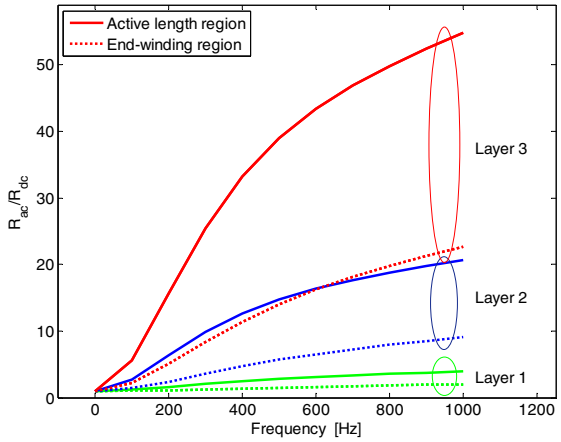

Fig. 7. R_{ac}/R_{dc} versus excitation frequency for winding temperature 20°C and excitation current 40A_{rms}

from the top/slot opening of the E-core assembly as shown in Fig. 1, i.e. coil layers 1 to 3. This allows for the flux leakage effects affecting the ac winding loss to be varied for the selected winding variants. Fig. 6 presents frequency variation of the winding loss generated in the hardware exemplar showing relatively good correlation between measured and calculated data. A small degree of discrepancy between the theoretical and experimental results for the 3-layer coil assembly is attributed here to uneven temperature distribution between the individual un-impregnated winding layers. The results confirmed that the ac winding loss is the most severe for the 3-layer coil arrangements. It is worth noting that the temperatures listed in Fig. 6 refer to the winding temperature. Also, the excitation current used across all the ac experiments/analyses was 40A_{rms}.

The 3-layer coil assembly has been chosen to illustrate the influence of winding loss separation on the temperature predictions, as the inhomogeneous winding loss distribution is expected to be the most prominent here. To demonstrate this, Fig. 7 compares the R_{ac}/R_{dc} ratio of the individual winding layers of the 3-layer coil with distinction made between the active and end-winding regions. It is clear that the top winding layer (layer 3) contributes significantly to the ac loss component as compared with the remaining layers.

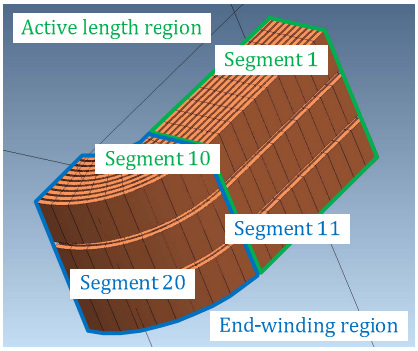

Fig. 8. FE model representation of the winding region subdivided into a number of smaller sections along the conductor length

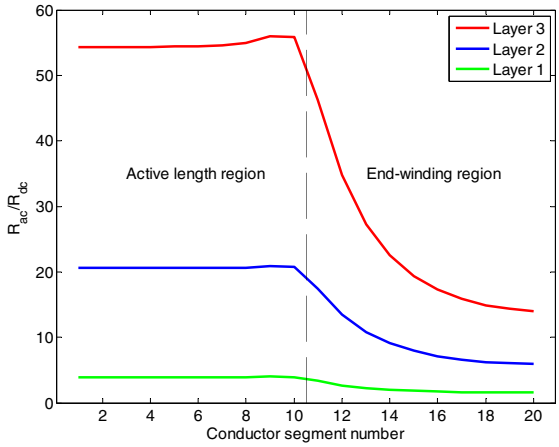

Fig. 9. R_{ac}/R_{dc} averaged per coil layers for the individual conductor segments versus conductor segment number, winding temperature 20°C, excitation current 40A_{rms} and excitation frequency 1kHz

In contrast, winding layer 1 is placed at the bottom of the slot and has the lowest ac loss contribution. It is important to note that for the analysed exemplar the ac loss is exaggerated due to the conductor arrangement, purposely selected here to encourage 'high' ac effects. The theoretical predictions suggest that the end-winding ac loss is non-negligible in this case and follows a trend, in which 'high'ac loss generated within the active length translate to 'high' ac end-winding loss. It has been suggested in the literature that this effect is attributed to the eddy-current return paths including a small portion of the end-winding [17]. It is assumed that the remaining length of the end-winding generates dc loss only. To provide an insight into the ac end-winding loss contribution a detailed FE model of the exemplar has been constructed, where an individual conductor is subdivided into a number of smaller sections along the conductor length for both the active length and end-winding regions. Fig. 8 presents FE model representation of the winding region with conductor segments 1 to 10 located in the middle and end of the winding active length respectively. Segments 11 to 20 represent end winding conductor sections placed in the nearest and furthest angular distance from the core pack respectively, Fig. 8. Fig. 9 shows R_{ac}/R_{dc} ratio derived for the individual conductor segments and averaged for the coil layers. The results indicate that the ac effects reduce when moving away from the laminated core pack for the end-winding conductor segments, Figs. 3 and 8. However, for the analysed exemplar, R_{ac}/R_{dc} does not decay to 1, which would

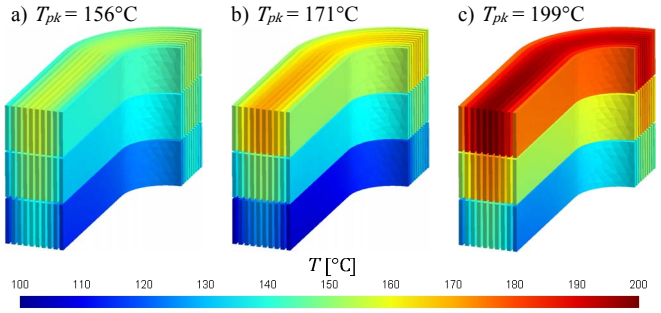

Fig. 10. Temperature distribution within the winding assembly from 3D thermal analysis a) power loss averaged per winding body – method I, b) power loss averaged per winding layers – method II, c) power loss averaged per winding conductors – method III; excitation current 40A_{rms}, excitation frequency 500Hz, cold plate temperature 20° C

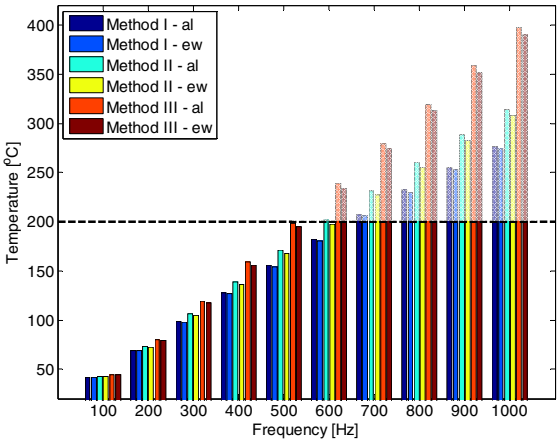

Fig. 11. Hot-spot active length and end-winding temperature vs. excitation frequency; excitation current 40A_{rms}, cold plate temperature 20°C; *al* – winding active length, *ew* – end-winding region

be the case if dc loss only was generated within the end-winding region. This indicates the complexity of the end-effects and suggests that the existing simplified methods for approximating the ac end-winding loss might not yield the required fidelity. The impact of the end-winding loss estimates on thermal behaviour of the analysed exemplar is discussed in the next section.

B. Exemplar – Thermal Behavior

Fig. 10 presents the temperature distribution within the winding assembly for the loss separation methods under consideration. The sinusoidal excitation current assumed in this example is equal to 40A_{rms}, and the excitation frequency is equal to 500Hz. The cold plate temperature is set to 20°C. The results indicate a prominent difference between the methods in terms of the absolute hot-spot temperature and location of the hot-spot. In all the cases the hot spot is located in the active length of the winding. The coarse loss separation (method I) under predicts the winding hot-spot temperature by 22% as compared with the most detailed approach considered in this analysis (methods III). When inspecting winding temperature distribution in the slot a characteristic shift of the slot hot-spot towards the slot-opening is evident for method III. This results from elevated ac winding loss at the slot-opening. Fig. 11 shows how the loss separating methods perform at various excitation frequencies. As expected, at dc and low frequencies all

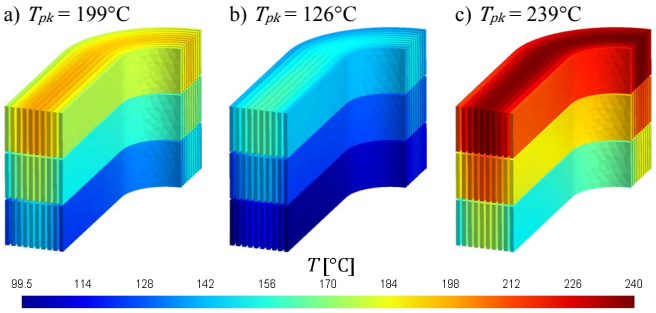

Fig. 12. Temperature distribution within the winding assembly from 3D thermal analysis a) end-winding ac loss accounted for – variant I, b) end-winding ac loss neglected assuming dc loss contribution only – variant II, c) end-winding loss from ac effects assumed to be equivalent to this for the active length – variant III; excitation current 40A_{rms}, excitation frequency 500Hz, cold plate temperature 20°C

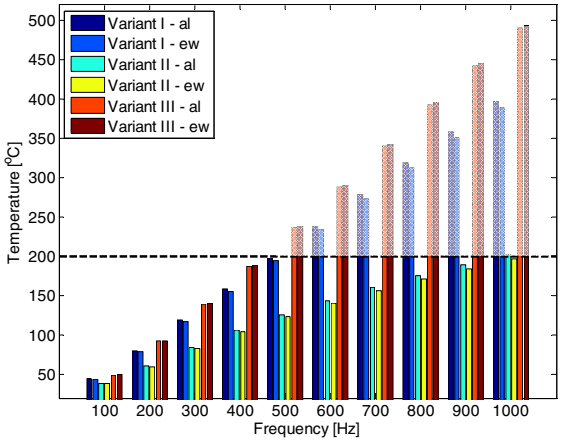

Fig. 13. Hot-spot winding temperature for the active length and end-winding regions vs. excitation frequency; excitation current 40A_{rms}, cold plate temperature 20°C

methods provide similar predictions for the hot-spot winding temperature. At higher excitation frequencies, where ac winding effects are more prominent, the discrepancy between the temperature predictions for the analysed loss separating methods is significant. Here, 35% discrepancy between method I and III has been recorded at the maximum operating frequency of 1kHz, considered in this comparison. The results suggest that the use of a detail winding loss definition is a prerequisite of accurate temperature predictions for design cases where the ac loss contribution is considerable. It is important to note that the temperature predictions, for the excitation frequency beyond 500Hz, exceed the winding insulation class (class N, 200°C) and have been included here to clearly illustrate the effects associated with the winding loss separation and definition in the thermal design-analysis of electrical machines.

Fig. 12 shows an example of the temperature distribution within the winding assembly obtained using the detailed approach (method III) for a number of differing approximation methods, of the end-winding ac loss contribution. Here, three variants are considered, variant I uses detailed end- winding loss data obtained from 3D FEAs, variant II assumes dc loss only for the end-winding $(R_{ac}/R_{dc})_{ew}$ = 1, and variant III assumes the end-winding ac loss effects to be equivalent to those in the active length region $(R_{ac}/R_{dc})_{ew} = (R_{ac}/R_{dc})_{al}$.

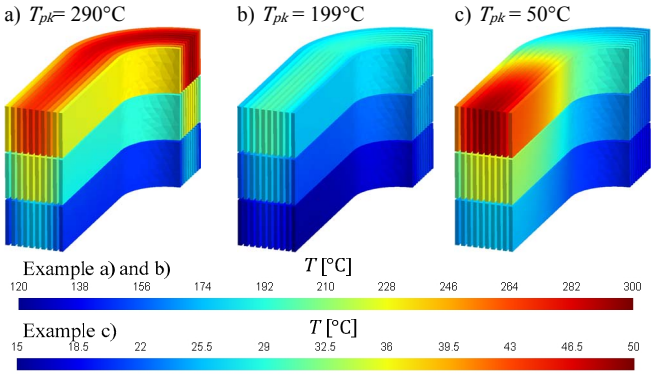

Fig. 14. Temperature distribution within the winding assembly from 3D thermal analysis a) natural convection passive heat extraction from the end-winding – variant I, b) active heat extraction by conduction from the end-winding to liquid cooled housing – variant II, c) enhanced active heat evacuation from the end-winding by spray cooling – variant III; excitation current 40A_{rms}, excitation frequency 500Hz, cold plate temperature 20°C

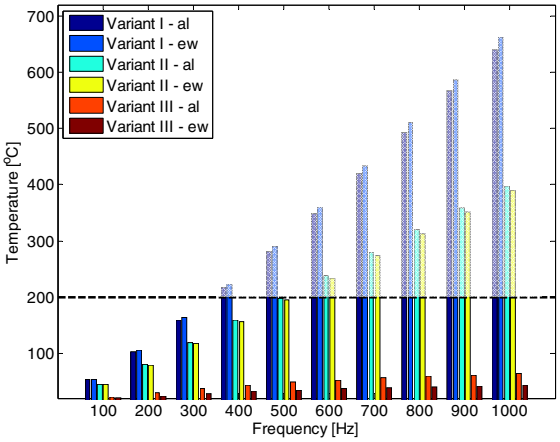

Fig. 15. Hot-spot winding temperature for the active length and end-winding regions vs. excitation frequency; excitation current 40A_{rms}, cold plate temperature 20°C

Note that the subscript *ew* and *al* refer here to the end-winding and active length respectively. The calculated results confirm the expected trends, with variant II under predicting and variant III over predicting the winding hots spot temperature as compared with the baseline variant I. Here, the discrepancy between temperature predictions is 37% for variant II and 20% for variant III. The discrepancy is particularly prominent for the cases where winding loss from ac effects is relatively 'high', Fig. 13. The results indicate that the location of the winding hot-spot is also being affected. Fig. 13 compares the hot-spot winding temperature for the active and end-winding regions showing that the absolute hot-spot temperature migrates from the active length to the end-winding region for the variants II and III respectively. These highlight the importance of appropriate end-winding loss treatment in thermal analysis, where significant ac winding effects are expected. As the hot-spot location is greatly affected by the end-winding loss contribution and thermal behavior.

The final illustration presents the effect of heat extraction technique from the end-winding region on the winding temperature distribution, Fig. 14. Here, three approaches commonly used in electrical machines are considered. Variant I with 'poor'/passive heat extraction is representative of a naturally cooled end-winding. Variant II with potted winding design, where heat generated in the end-winding is transferred/conducted to the liquid cooled housing, is an example of 'average'/active dissipative heat evacuation. Finally, variant III represents a spray cooling approach with 'good'/enhanced-active heat extraction from the end-winding regions. Heat extraction from the active winding is assured by the liquid cooled housing for all the analysed variants. The heat transfer coefficients for variants I and III have been assumed as 5W/m^{2}K and 750W/m^{2}K respectively [22]. It is important to note that detailed loss data has been used for all the variant heat extraction techniques from the end-winding region.

The benefits of improved heat extraction from the end-winding region are clear with 31% improvement for heat extraction variant II and 83% variant III when comparing the absolute hot-spot temperatures for passive heat extraction form the end-winding (variant I), Fig. 14. Fig. 15 illustrates the influence of the elevated ac loss on the winding hot-spot temperature. Again, migration of the absolute hot-spot winding temperature is present both for the heat extraction method and operation point. For example, the hot-spot location changes from the active winding to end region for higher excitation frequencies, when comparing the end-winding heat extraction variant I with variant II and III. Also, for the analysed exemplar, the active heat evacuation from end-winding sets the hot-spot location to the winding active length. These effects are particularly important in thermal design when deciding on heat extraction methods and also for monitoring purposes to assure machine 'safe'/'healthy' operation.

V. Conclusions

The results suggest that a more detailed winding loss definition is essential for accurate temperature predictions for devices, where localised winding power loss is expected to be significant. However, to account for the localised winding power loss effects, an improved fidelity thermal modelling approach is required. Both the thermal model definition/formulation and power loss data need to accommodate for the more detailed or higher resolution modelling approach. Application of the more complex model definition as discussed earlier, e.g. individual conductors are accounted for in the analysis, is demanding in terms of the model preparation/set up and solving time. An approach providing a compromise between the model complexity and solution accuracy makes use of the layer averaged winding power loss separation. The theoretical findings suggest that this approach (method II) provides temperature predictions closer to that obtained from method III. It is important to note that the layer averaged winding loss separation method is not limited to devices, where the distinct physical layer coil/winding arrangement is present. In general, the layer loss separation method refers to the winding sub-regions or layers with distinct power loss generation.

Analysis of ac power loss for the end-winding region requires the use of 3D FEA. As the 3D FE modelling approach is time consuming and might not be available, various assumptions regarding the end-winding loss at ac operation are usually made, e.g. dc end-winding loss is

present only $(R_{ac}/R_{dc})_{ew} = 1$ or end winding ac effects are equivalent to these present in the winding active length $(R_{ac}/R_{dc})_{ew} = (R_{ac}/R_{dc})_{al}$. Here, the results indicate that neither of the simplified approaches of approximating end-winding loss is adequate in thermal analysis, in particular when the overall winding ac effects within the analysed machine are prominent. For thermal analysis, where the winding ac loss is expected to be 'low', the assumption of dc end-winding loss only provides relatively 'good' approximation for the temperature predictions in the analysed exemplar.

When examining results from analysis of alternative techniques of heat transfer from the end-winding, it is evident that spray cooling (variant III) provides superior heat extraction as compared with the alternative solutions, e.g. naturally cooled (variant I) or active heat removal trough the liquid cooled housing (variant II). The theoretical predictions indicate that the location of the winding hot spot is affected by the method in which the heat is evacuated from the end-winding region. Here, the hot spot migrates from the end-winding region (variant I) to the active length region (variant II and III). This is particularly important in thermal design-analysis of electrical machines, where a reduced order modeling approach is adopted in order to assure machine design in a timely manner. Also, when making decisions related to instrumenting machine with thermal sensors.

VI. Acknowledgment

The University of Bristol wish to thank Infolytica Europe for providing the software used in this research.

VII. References

[1] A. Boglietti, A. Cavagnino, D. Staton, M. Shanel, M. Mueller, C. Mejuto, "Evolution and Modern Approaches for Thermal Analysis of Electrical Machines," *IEEE Transactions on Industrial Electronics*, vol. 56, no. 3, pp. 871-882, March 2009.

[2] D. Staton, A. Boglietti, A. Cavagnino, "Solving the More Difficult Aspects of Electric Motor Thermal Analysis in Small and Medium Size Induction Motors," *IEEE Transaction on Energy Conversion*, vol. 20, no. 3, pp. 620 -628, September 2005.

[3] A. Boglietti, A. Cavagnino, D. M. Ionel, M. Popescu, D. A. Staton, S. Vaschetto, "A General Model to Predict the Iron Losses in PWM Inverter-Fed Induction Motors," *IEEE Transactions on Industry Applications*, vol. 46, no. 5, pp. 1887-1890, September/October 2010.

[4] P. H. Mellor, D. Roberts, D. R. Turner, "Lumped Parameter Thermal Model for Electrical Machines of TEFC Design," *Electric Power Applications*, *IEE Proceedings B*, vol. 138, no. 5, pp. 205-218, September 1991.

[5] C. Mejuto, M. Mueller, M. Shanel, A. Mebarki, M. Reekie, D. Staton, "Improved Synchronous Machine Thermal Modelling," *18th International Conference on Electrical Machines*, *(ICEM 2008)*, Vilamoura, Portugal, pp. 1-6, 6-9 September.

[6] R. Wrobel, A. Mlot, P. H. Mellor, **"**Contribution of End-Winding Proximity Losses to Temperature Variation in Electromagnetic Devices," *IEEE Transactions on Industrial Electronics*, vol. 59, no. 2, pp. 848-857, February 2012.

[7] N. Simpson, R. Wrobel, P. H. Mellor, "Estimation of Equivalent Thermal Parameters of Impregnated Electrical Windings," *IEEE Transactions on Industry Applications*, vol. 49, no. 6, pp. 2505-2515, November/December 2013.

[8] N. Simpson N., R. Wrobel, P. H. Mellor, "An Accurate Mesh Based Equivalent Circuit Approach to Thermal Modelling," *IEEE Transactions on Magnetics*, vol. 50, no. 2, pp. 1-4, February 2014.

[9] R. Wrobel, D. Salt, A. Griffo, N. Simpson, P. H. Mellor, "Derivation and Scaling of AC Copper Loss in Thermal Modeling of Electrical Machines," *IEEE Transactions on Industrial Electronics*, vol. 61, no. 8, pp. 4412-4419, August 2014.

[10] R. Wrobel, P. H. Mellor, D. Holliday, "Thermal Modelling of a Segmented Stator Winding Design," *IEEE Transactions on Industry Applications*, vol. 47, no. 5, pp. 2023-2030, September/October 2011.

[11] R. Wrobel, P. H. Mellor, N. McNeill, D. A. Staton, "Thermal Performance of an Open-Slot Modular-Wound Machine with External Rotor," *IEEE Transactions on Energy Conversion*, vol. 25, no. 2, pp. 403-411, June 2010.

[12] R. Wrobel, D. Staton, R. Lock, J. Booker, D. Drury, "Winding Design for Minimum Power Loss and Low-Cost Manufacture in Application to Fixed-Speed PM Generator," *IEEE Transactions on Industry Applications*, vol. 51, no. 5, pp. 3773-3782, September/October 2015.

[13] R. Wrobel, P. H. Mellor, **"**A General Cuboidal Element for Three-Dimensional Thermal Modelling," *IEEE Transactions on Magnetics*, vol. 46, no. 8, pp. 3197-3200, August 2010.

[14] R. Wrobel, P. H. Mellor, "Thermal Design of a High Energy Density Wound Components," *IEEE Transactions on Industrial Electronics*, vol. 58, no. 9, pp. 4096-4104, September 2011.

[15] R. Wrobel, P. H. Mellor, M. Popescu, D. A. Staton, "Power Loss Analysis in Thermal Design of Permanent Magnet Machines – A Review," *IEEE Transactions on Industry Applications*, (early access article).

[16] P. H. Mellor, R. Wrobel, D. Salt, A. Griffo, "Experimental and Analytical Determination of Proximity Losses in a High-Speed PM Machine," *IEEE Energy Conversion Congress and Exposition*, *(ECCE 2013)*, Denver, Colorado, USA, pp. 3504-3511, 15-19 September 2013.

[17] P. H. Mellor, R. Wrobel, N. Simpson, "AC Loss in High Frequency Electrical Machine Windings Formed from Large Section Conductors," ," *IEEE Energy Conversion Congress and Exposition*, *(ECCE 2014)*, Pittsburgh, Pennsylvania, USA, pp. 5563-5570, 14-18 September 2015.

[18] R. Wrobel, N. Simpson, P. H. Mellor, J. Goss, D. A. Staton, "Design of a Brushless PM Starter-Generator for Low-Cost Manufacture and a High-Aspect-Ratio Mechanical Space Envelope ," *IEEE Energy Conversion Congress and Exposition*, *(ECCE 2015)*, Montreal, Quebec, Canada, pp. 813-820, 20-24 September 2015.

[19] M. Vetuschi, F. Cupertion, "Minimization of Proximity Losses in Electrical Machines with Tooth Wound Coils," *IEEE Transactions on Industry Applications*, vol. 51, no. 4, pp. 3068-3076, July/August 2015.

[20] D. C. Hanselman and W. H. Peake, "Eddy-currents Effects in Slot-Bound Conductors," *Proc. Inst. Elect. Eng.—Electr. Power Appl.*, vol. 142, no. 2, pp. 131–136, Mar. 1995.

[21] F. Qi, M. Schenk, R. W. De Doncker, "Discussing Details of Lumped Parameter Thermal Modeling in Electrical Machines," *7th IET International Conference on Power Electronics, Machines and Drives*, *(PEMD 2014)*, pp. 1-6, Manchester, UK, 8-10 April 2014.

[22] http://www.motor-design.com/cmsAdmin/uploads/end_winding_spray_cooling_model.pdf (Motor-CAD End-Winding Spray Cooling Model).

VIII. Biographies

Rafal Wrobel (SM'13) received the M.Sc.Eng. degree from the Technical University of Opole, Opole, Poland, in 1998, the Ph.D. degree from the Technical University of Lodz, Lodz, Poland, in 2000 and the Habilitation degree from the Technical University of Opole, Opole, Poland, in 2013. (2000-2002), he was an Assistant Professor with the Technical University of Opole. (2002-2011) he was a Research Fellow with the Electrical Energy Management Group (EEMG) at the University of Bristol, Bristol, U.K. Since 2011, he has been a Senior Research Fellow with the EEMG, and his research interests include multi-physics and multi-disciplinary design-analysis of electrical machines and wound passive components.

Nick Simpson received the B.Eng. and Ph.D. degrees in electrical engineering from the Department of Electrical and Electronic Engineering, University of Bristol, Bristol, U.K., in 2009 and 2014, respectively. He is currently a Lecturer in electrical engineering at the University of Bristol. His research activities include the modelling, manufacture and characterisation of electrical machines and wound passive components, primarily for more electric aircraft and electric vehicle applications.